Bull Volcanol (2016) 78: 71
DOI 10.1007/s00445-016-1064-x

RESEARCH ARTICLE

Magma decompression rates during explosive eruptions of Kīlauea volcano, Hawaii, recorded by melt embayments

David J. Ferguson[1,2,7] · **Helge M. Gonnermann**[3] · **Philipp Ruprecht**[1,8] · **Terry Plank**[1] · **Erik H. Hauri**[4] · **Bruce F. Houghton**[5] · **Donald A. Swanson**[6]

Received: 23 January 2016 / Accepted: 5 September 2016 / Published online: 22 September 2016

Abstract The decompression rate of magma as it ascends during volcanic eruptions is an important but poorly constrained parameter that controls many of the processes that influence eruptive behavior. In this study, we quantify decompression rates for basaltic magmas using volatile diffusion in olivine-hosted melt tubes (embayments) for three contrasting eruptions of Kīlauea volcano, Hawaii. Incomplete exsolution of H_2O, CO_2, and S from the embayment melts during eruptive ascent creates diffusion profiles that can be measured using microanalytical techniques, and then modeled to infer the average decompression rate. We obtain average rates of ~0.05–0.45 MPa s^{-1} for eruptions ranging from Hawaiian style fountains to basaltic subplinian, with the more intense eruptions having higher rates. The ascent timescales for these magmas vary from around ~5 to ~36 min from depths of ~2 to ~4 km, respectively. Decompression-exsolution models based on the embayment data also allow for an estimate of the mass fraction of pre-existing exsolved volatiles within the magma body. In the eruptions studied, this varies from 0.1 to 3.2 wt% but does not appear to be the key control on eruptive intensity. Our results do not support a direct link between the concentration of pre-eruptive volatiles and eruptive intensity; rather, they suggest that for these eruptions, decompression rates are proportional to independent estimates of mass discharge rate. Although the intensity of eruptions is defined by the discharge rate, based on the currently available dataset of embayment analyses, it does not appear to scale linearly with average decompression rate. This study demonstrates the utility of the embayment method for providing quantitative constraints on magma ascent during explosive basaltic eruptions.

Keywords Basaltic volcanoes · Magma decompression rates · Melt embayments

Editorial responsibility: P. Allard

Electronic supplementary material The online version of this article (doi:10.1007/s00445-016-1064-x) contains supplementary material, which is available to authorized users.

✉ David J. Ferguson
d.j.ferguson@leeds.ac.uk

[1] Lamont-Doherty Earth Observatory, Columbia University, Palisades, NY 10964, USA

[2] Department of Earth and Planetary Sciences, Harvard University, Cambridge, MA 02138, USA

[3] Department of Earth Science, Rice University, Houston, TX 77005, USA

[4] Department of Terrestrial Magnetism, Carnegie Institution of Washington, Washington, DC 20015, USA

[5] Department of Geology and Geophysics, University of Hawaii at Manoa, Honolulu, HI 96822, USA

[6] U. S. Geological Survey, Hawaiian Volcano Observatory, Hawaii National Park, HI 96718, USA

[7] Present address: School of Earth and Environment, University of Leeds, Leeds LS2 9JT, UK

[8] Present address: Department of Geological Sciences, University of Nevada, Reno, NV 89557, USA

Introduction

At basaltic volcanoes, where magma viscosities are relatively low, explosive eruptions occur over a wide range of mass discharge rates or equivalently eruptive intensities (e.g., Houghton and Gonnerman 2008). A key goal of volcanology is to gain an understanding of the processes that control the dramatic differences in eruptive intensity and thereby enhance our ability to forecast the style of an impending eruption. During explosive eruptions, magmas that were previously stored in presumably pressurized reservoirs flow upwards through a volcanic conduit in which fragmentation occurs, transitioning the magma from a continuous melt phase with a large volume fraction of suspended CO_2-H_2O-SO_2 fluid or vapor bubbles to a continuous and rapidly expanding gas phase with suspended pyroclasts of bubbly magma (Woods 1995; Cashman and Sparks 2013). The style of basaltic explosive eruptions is thought to be predominantly dependent on the magma ascent velocity, which asserts a strong control on the movement and spatial distribution of the magmatic vapor (e.g., Wilson and Head 1981; Parfitt and Wilson 1995; Parfitt 2004; Goepfert and Gardner 2010), and in turn affects the fluid dynamics and fragmentation of the erupting magma (Vergniolle and Jaupart 1986; Parfitt 2004; Houghton and Gonnermann 2008; Namiki and Manga 2006; Gonnermann 2015). The presence of pre-existing exsolved volatiles (i.e., prior to the initiation of eruptive ascent) also has the potential to modulate the fluid dynamics of the magma (e.g., Vergniolle and Jaupart 1986) and in addition affects magma density and, hence, magmastatic pressure conditions within the eruptive conduit.

The height to which the fragmented magma is ejected above the volcanic vent, which ultimately determines the environmental and societal impact of an eruption, is approximately proportional to the fourth root of the discharge rate (Pyle 2015). These rates, inferred from tephra dispersal, are often used as observational constraints on models of the conditions of eruptive ascent and for estimates of decompression rates in the volcanic conduit (Mastin 2002). However, although they are interrelated parameters, decompression and discharge rates do not necessarily scale linearly, for example, because of viscous stresses and/or differences in conduit geometry. For historical eruptions, where discharge rates and height of the eruptive jet/column have been observed, these observations do not therefore provide direct information on the conditions of magma ascent at depth. This is also because near-surface geometries of the eruptive conduit/vent may not reflect those at depth (Parcheta et al. 2015). Furthermore, at some volcanoes, such as Kīlauea, there is evidence for past explosive eruptions that have no historically observed equivalent in intensity (e.g., Swanson et al. 2012, 2014; May et al. 2015) and the conditions that accompany such intensely explosive eruptions remain largely unresolved. Since a number of important processes are directly dependent on the decompression rate, such as bubble nucleation, bubble growth, and fragmentation itself (Parfitt and Wilson 1995; Mangan and Cashman 1996; Mangan et al. 2014; Gonnermann 2015), robust constraints on this parameter will enable a fuller understanding of the processes that determine the intensity of explosive eruptions driven by magmatic volatiles. The average decompression rate between magma storage reservoir and surface should also provide information about the potential presence of abundant pre-existing exsolved volatiles. The aim of this study is to begin this task of seeking independent constraints on magma decompression rates for basaltic eruptions with distinctly different eruption intensities.

Previous estimates of magma decompression rates have been made using numerical models (Mastin 2002), laboratory experiments (Namiki and Manga 2006, 2008; Goepfert and Gardner 2010), and physical observations of the erupted material, such as crystal textures (Toramuru et al. 2008; Suzuki and Fujii 2010; Wright et al. 2012); but these are limited by issues associated with constraining unknown parameters, such as conduit dimensions, mass discharge rates, crystallization conditions, and/or magma overpressure. A more direct method is to determine the rates of time-dependent chemical reactions that occur as magmas rise beneath volcanoes, such as crystal-melt reactions (e.g., Rutherford and Hill 1993; Castro and Dingwell 2009), intra-crystal diffusion (e.g., Costa and Dungan 2005; Ruprecht and Plank 2013), or the loss of dissolved volatile components during vesiculation (Liu et al. 2007; Humphreys et al. 2008; Lloyd et al. 2014). Such geochemical chronometers have the potential to provide independent information on processes occurring at rates relevant to magma ascent and eruption. In this study, we apply the latter of these, volatile diffusion through ascending melts, to infer rates of syn-eruptive decompression for three eruptions of Kīlauea (Fig. 1) of varying style and intensity. Our results are based on compositional profiles measured along small tubes of melt (embayments) contained within olivine crystals, which are not only recorders but also timekeepers of decompression-volatile exsolution.

Melt embayments and choice of samples

Melt embayments are elongate pockets or tubes of melt that become partially enclosed within growing crystals (Liu et al. 2007) (Fig. 2). Unlike more common melt inclusions, which are entirely enclosed, embayments remain open at the crystal edge, thereby allowing chemical exchange with the external magma. During ascent, decompression of magma leads to a drop in the solubility of dissolved volatiles, primarily H_2O, S, and CO_2, and bubble growth occurs by volatile exsolution. In the case of an embayment that is being carried upwards in a magma from which dissolved volatiles are being exsolved, the volatile components have to diffuse along the length of the

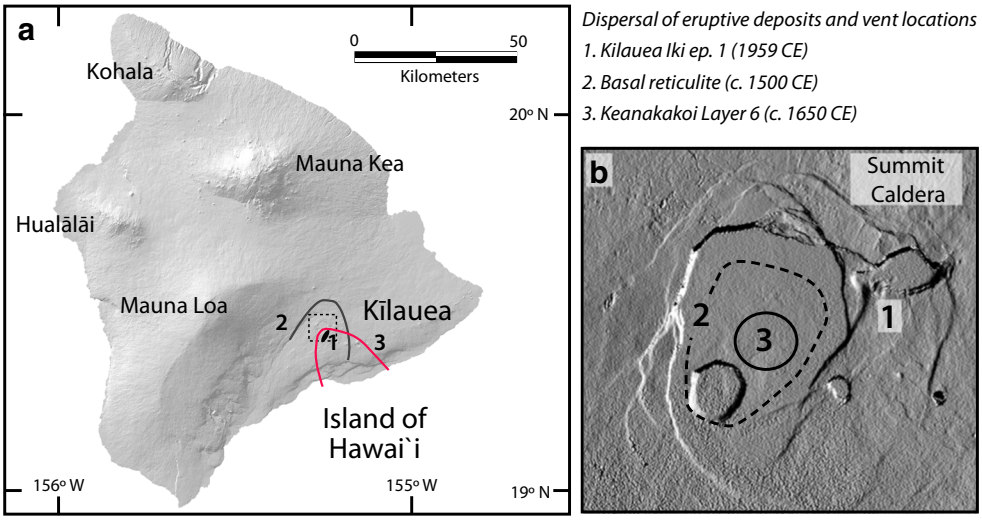

Fig. 1 DEM of the Island of Hawaii (*A*), with its five shield volcanoes, and Kīlauea's summit caldera (*B*). *Curved lines* on the map in *A* show the dispersal of pyroclasts from the three eruptions studied here. The area of panel *B* is marked by the *dashed box*. This shows the locations of the vents/fissures for each eruption. *1*: site of 1959 Kīlauea Iki eruption from a vent on the caldera rim. *2*: interpreted buried ring fault (*dashed line*) from which the c. 1500 CE reticulite was erupted (May et al. 2015). *3*: circle surrounding approximate site of c. 1650 CE subplinian eruption. Elevation data from http://www.soest.Hawaii.edu

embayment towards growing bubbles. For embayments with bubbles attached to the embayment mouth, this diffusion, while a consequence of the drop in solubility during decompression, is driven by the concentration of dissolved volatiles at the melt-bubble interface, a direct function of vapor pressure inside the bubble. The diffusivities of H_2O, CO_2, and S in silicate melts are sufficiently small to prevent the attainment of equilibrium concentrations within embayments that have lengths on the order of 100 μm for a wide range of decompression rates (e.g., Lensky et al. 2004; Gonnerman and Manga 2005; Pichavant et al. 2013; Zhang et al. 2007, 2010). Consequently, distinct diffusion-controlled concentration profiles may be preserved within an embayment, allowing the estimation of decompression rates via diffusion modeling (Liu et al. 2007). Previous studies have applied this method to silicic (Liu et al. 2007; Humphreys et al. 2008) and basaltic-andesitic (Lloyd et al. 2014) eruptions. Here, we extend this method to a basaltic volcano.

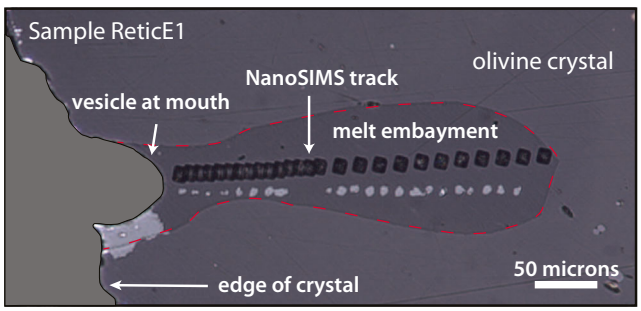

Fig. 2 Olivine-hosted melt embayment from Kīlauea (sample ReticE1). The melt (now glass) tube or embayment is partly enclosed within an olivine crystal that was carried with the erupted magma. *Marks* on the glass are from the NanoSIMS microbeam analysis (<10 μm raster) used to measure volatile concentrations along the embayment glass and from the electron microprobe analysis (*smaller spots*)

We present data for four embayments from three contrasting summit eruptions of Kīlauea. These are (1) 1959 Kīlauea Iki episode 1 (embayment IkiE1). This was the initial episode of the archetypal Hawaiian-style eruption in 1959, which involved fountain heights of up to 370 m (Eaton et al. 1987), the highest observed in the modern era. We chose the first episode of the 1959 eruption because subsequent phases were affected by the drain-back of degassed lava into the conduit (Wallace and Anderson 1998; Sides et al. 2014a). Our samples are taken from layer ρ17 of Stovall et al. (2011). (2) The Keanakāko'i basal reticulite (embayments ReticE1 and ReticE2): a thick reticulite-pumice layer formed from an eruption in c. 1500 CE (Swanson et al. 2012; May et al. 2015), which is present on all sides of Kīlauea Caldera and is more widely dispersed than deposits from any historical high-fountaining eruption. Ascent and mass discharge rates for this deposit are probably larger than for any historical eruption, with fountain heights exceeded 600 m. The reticulite offers a picture of unusual eruption dynamics because its distribution is only consistent with a series of widely spaced vents around the rim of the caldera (May et al. 2015). (3) The Keanakāko'i layer 6 deposit (embayment KeaE1): layer 6 of McPhie et al. (1990), which is a widespread scoria fall deposit from an eruption in c. 1650 CE, thought to be a subplinian scale event. This deposit can be mapped to the coast (20 km distant), and its southeastward dispersal direction implies columns that extended into the jet stream, most likely to >12 km. Despite the high intensity, this eruption had a relatively small volume of c. 0.02 km^3 (Swanson et al. 2012). None of these eruptions show evidence for the involvement of external groundwater

and so were all driven by magmatic volatiles. All measurements were made on embayments found in loose olivine crystals hand-picked from fall deposits.

Geochemical analysis

The concentrations of five volatile species (H_2O, CO_2, S, F, and Cl) were measured along rapidly quenched (sideromelane) melt embayments by secondary ion mass spectrometry (SIMS) using a Cameca IMS 6f SIMS and Cameca NanoSIMS 50L at the Department of Terrestrial Magnetism, Carnegie Institution of Washington, following methods described in Saal et al. (2008) and Hauri et al. (2011). The NanoSIMS technique is particularly useful for this work as it enables precise measurement of multiple analytes at very small spatial scales (Saal et al. 2008; Hauri et al. 2011) (spot size <10 μm; Fig. 2) and therefore at a resolution relevant to volatile diffusion length-scales (typically 100–200 μm). The internal precision of the NanoSIMS data can be assessed from the compositional plateaux of the longer embayments (i.e., ReticE1 and KeaE1), which give 2RSD values (RSD = (standard deviation/mean) × 100) of ≤3 % for H_2O, CO_2, and Cl, 1 % for S, and 2 % for F. Based on replicate analyses of an internal glass standard (MR-ND-7001; Table 3 in spreadsheet), we obtain 2RSD values for the SIMS analysis of 4 % for CO_2, 6 % for H_2O, 2 % for S, 4 % for F, and 6 % for Cl. Analysis of MR-ND-7001 by both methods shows an agreement between techniques of <3 % for H_2O, CO_2, and S, 9 % for F and 3 % for Cl.

Major element concentrations in the embayment glasses and host olivines were measured by electron microprobe (EMPA) at the American Museum of Natural History in New York using a Cameca SX100 microprobe. Analyses were performed with an accelerating voltage of 15 kV, 20 nA probe current (6 nA for K and Na), and beam size of 5 μm. All elements were routinely measured for 20–30 s. Volatile and major element data for the embayments can be found in the accompanying spreadsheet.

Diffusion modeling

Our diffusion modeling is based on compositional profiles of H_2O, CO_2, and S for four embayments (Fig. 3), all of which are consistent with syneruptive diffusion of volatiles into bubbles that are preserved as vesicles at the embayment outlets (Fig. 2). We constrained the timescales of volatile diffusion using a 1-D diffusion model with boundary conditions and diffusivities that evolve as the magma ascends and exsolves its volatile constituents.

The free parameters in the model are (1) the initial dissolved volatile concentration in the melt (C^o_{H2O}, C^o_{CO2}, and C^o_S); (2) the final pressure prior to quenching of the glass (P_f); (3) the mass fraction of exsolved volatiles prior to decompression (M^o); and (4) the decompression rate (dP/dt), assumed constant with time. When modeling equilibrium volatile exsolution, the initial volatile concentrations in the embayment are assumed to be in equilibrium at the pressure at which ascent is initiated. Basaltic magmas typically become volatile saturated at lower crustal pressures, exsolving a CO_2-rich phase (Newman and Lowenstern 2002). It is therefore important to include the mass fraction of "pre-existing" exsolved volatiles (present as a supercritical fluid or vapor) in the model, not only because its existence and significance remains a matter of debate (Vergniolle and Jaupart 1986; Allard et al. 2005; Houghton and Gonnerman 2008) but also because it will affect H_2O-CO_2 solubilities (e.g., Gonnermann and Manga 2005). At the concentrations typically found in Hawaiian magmas, H_2O and S are only exsolved in significant amounts at relatively low pressures (i.e., <30 MPa; Witham et al. 2012) and this pre-existing fluid is therefore predominantly composed of CO_2. As such, the initial concentration of dissolved CO_2 in the embayment melt (C^o_{CO2}) and the initial pressure are interrelated parameters. Because the three major volatile species have significantly different diffusivities and solubilities, we can multiply constrain the decompression rate by modeling the diffusion profiles for all three volatile species simultaneously. To find the best-fitting decompression rate, we performed a grid-search for each embayment, in which the free parameters listed above were varied independently to find the minimum root mean square (RMS) error between the model and our data (Fig. 3 and Supplementary Material Figs S1–S4).

The initial concentrations of H_2O, CO_2, and S are relatively well constrained for most embayments, because they are close to the values measured in the embayment interior at large distances from the embayment mouth. In the case of embayment IkiE1, which is too short to preserve the initial H_2O concentrations, we also include constraints from analyses of melt inclusions (Sides et al. 2014a). We assume that the embayments were at equilibrium prior to eruption, implying that H_2O, CO_2, and S concentrations were initially constant along the length of the embayment. We used the solubility model of Dixon (1997) for H_2O and CO_2 to determine the pressure and co-existing exsolved volatile phase composition at the specified initial concentrations, and we used the solubility model of Witham et al. (2012) to determine corresponding S solubilities. Conceptually, these initial conditions represent the conditions of pre-eruptive magma storage. Pressure (P) is assumed to decrease due to eruptive magma ascent at a constant rate from the initial value. Although decompression rate (dP/dt) was probably not constant throughout the ascent of any given melt embayment, the assumption of a constant dP/dt minimizes the number of model parameters. The value of

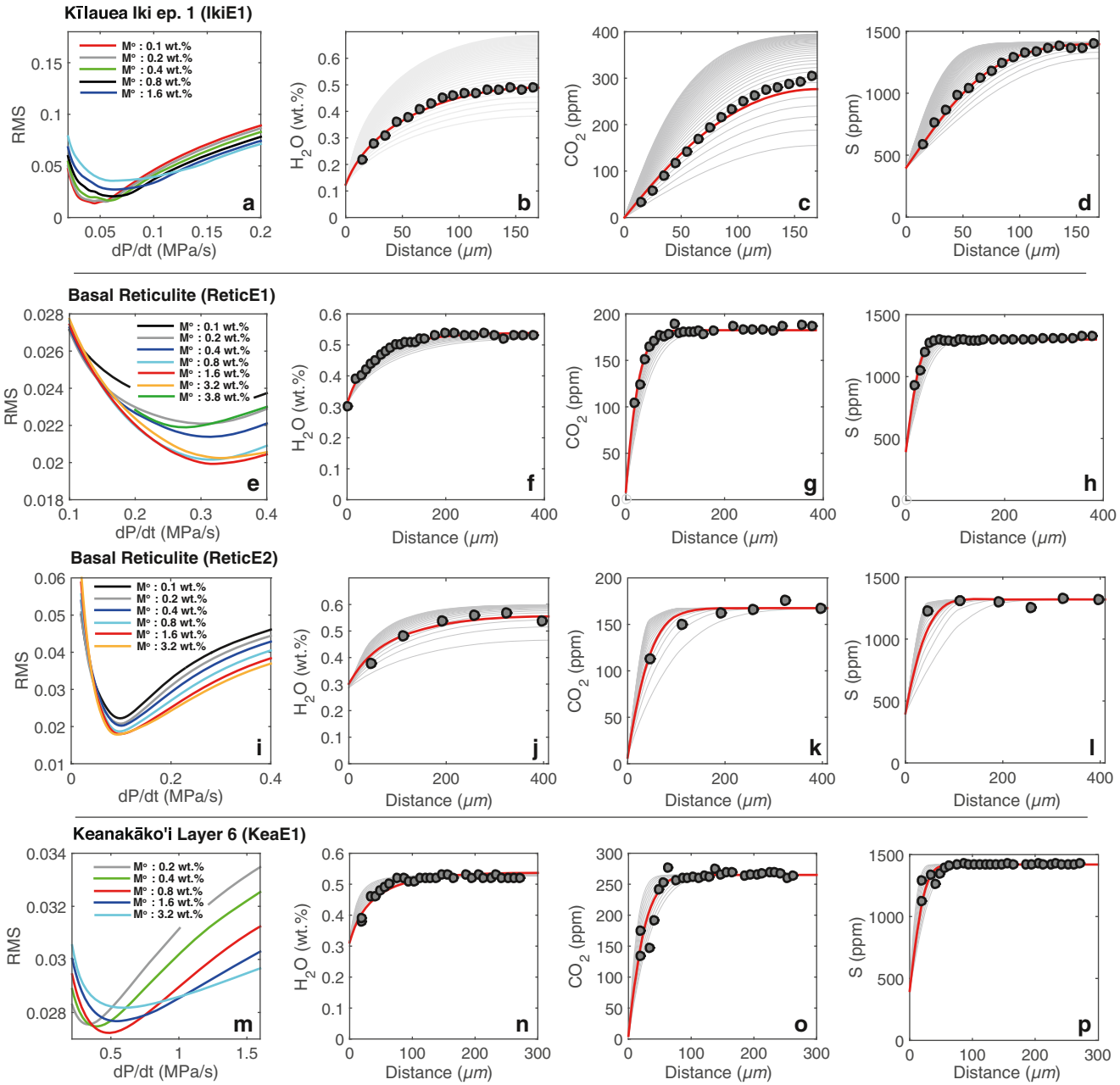

Fig. 3 Results from analysis and diffusion modeling of H_2O, CO_2, and S in melt embayments from explosive eruptions of Kīlauea: **a-d** Kīlauea Iki (IkiE1); **e**–**h** c. 1500 Reticulite (ReticE1); **i**–**l** c. 1500 Reticulite (ReticE2); **m**–**p** Keanakāko'i Layer 6 (KeaE1). The first panel in each *row* shows the root mean square error versus decompression rate for ascent models with different amounts of pre-existing exsolved volatiles (note the change in the scale of the *x*-axis for each). The next three panels show the measured H_2O, CO_2, and S contents (*gray circles*) along the embayment and profiles from the best-fit model (*red lines*) using the parameters listed in Table 2. The embayment outlet (i.e., melt-bubble interface) is plotted at distance = 0. The sensitivity of the modeled profiles to changes in the decompression rate are illustrated by the *gray lines*, which show the results from models using the same best-fit parameters but with *dP/dt* values that cover the range used in the grid-search (listed in Table 1). For plots showing the full results of the grid search for all the parameters modeled, see Supplementary Material Figs. 1-4

dP/dt obtained through our analysis thus represents a characteristic average value, given various simplifying assumptions.

Observations indicate that a vesicle was attached to the mouth of each melt embayment (e.g., as visible in Fig. 2). We therefore treat this bubble plus melt embayment as our "system" and are not concerned about the conduit-scale fluid dynamics of magma ascent. For the ranges of decompression rates under consideration, and probable magma viscosities, the characteristic viscous time scale (τ_{vis}) is much shorter than the characteristic decompression time scale (τ_{dec}) so that it is reasonable to assume that upon decompression the pressure inside the bubble remained close to ambient pressure (P) (e.g.,

Gonnermann and Manga 2007, and references therein). Furthermore, we assume that the concentration of each species at the melt-exsolved fluid/vapor interface is determined by the equilibrium solubility at P (e.g., Proussevitch et al. 1993) for a given composition of the exsolved volatile phase. Consequently, as P decreases the concentration of dissolved H_2O, CO_2 and S at the embayment mouth will also decrease. This results in a concentration gradient during magma ascent that causes diffusion of H_2O, CO_2, and S from the interior of the embayment into the bubble. The initial mass of exsolved volatiles inside the bubble is an independent parameter, and the vapor/fluid composition was determined from the solubility models at the given initial concentrations of dissolved H_2O, CO_2, and S (Dixon 1997; Witham et al. 2012). The vapor/fluid composition during the decompression was calculated using mass balance, under the assumption that the bubble at the embayment mouth was representative of bubbles throughout the magma and that these are always in equilibrium with the surrounding melt. Conceptually, the concentration boundary condition for the melt embayment is therefore representative of the conditions of the magma at large. Because of bubble mobility, it is possible that the bubble attached to a given olivine crystal may have originated elsewhere. Furthermore, it is difficult to reconstruct the three-dimensional geometry of melt surrounding the bubble and olivine. Therefore, the mass of exsolved volatiles inside the bubble, relative to the mass of melt from which volatiles will diffuse into the bubble upon eruptive ascent, is undetermined. To address this uncertainty, we have assumed different mass fractions of volatiles inside the bubble, relative to the mass of melt from which they exsolve. We refer to this as the initial or pre-eruptive exsolved volatiles, denoted by M^o.

The embayments are three-dimensional elongate volumes. Their length is measured from mouth to interior and is longer than their width. Because diffusion would have been predominantly along this direction, the diffusion calculations were performed in one dimension, with χ denoting the distance from the embayment mouth ($\mathcal{X} = 0$) to the interior embayment terminus ($\mathcal{X} = L$). The governing one-dimensional partial differential equation is the diffusion equation, given by

$$\frac{\partial C_i}{\partial t} = \frac{\partial}{\partial x}\left(D_i \frac{\partial C_i}{\partial x}\right) \quad (1)$$

This equation was solved for each volatile (i) as a system of ordinary differential equations using a stiff ODE solver as implemented in the function pdepe of Matlab®. For diffusivities of H_2O, CO_2, and S, we used the formulations of and Freda et al. (2005), respectively. In other words, $D_i = D_i(\mathcal{X}, t)$ and dependent on temperature, pressure, and H_2O. Initial concentrations of H_2O, CO_2, and S were constant throughout the model domain, that is $C_i(\mathcal{X}, t = 0) = C_i^0$ for all values of χ. For the diffusion calculation, a Dirichlet boundary condition (concentration) was specified at the embayment mouth and a Neumann boundary condition (no flux) at the far end of the embayment. That is, C_i $(\mathcal{X} = 0, t > 0)$ is specified and $\partial C_i(\mathcal{X} = L, t > 0)/\partial\mathcal{X} = 0$. The specified concentration at the embayment mouth corresponds to the equilibrium solubility of each volatile species at pressure P and the exsolved volatile composition corresponding to an equilibrium between bubble and surrounding mass of melt (Dixon 1997). The extent to which exsolution will continue at low pressures (i.e., upon eruption) depends on how quickly the magma is quenched. Analyses of matrix glasses near the embayment mouths shows differing H_2O concentrations in the quenched glass between eruptions (0.1 wt% in Kīlauea Iki versus 0.3 wt% in the Reticulite and Layer 6 glasses). We therefore specify the final boundary condition during decompression (i.e., at P_f) to match this observed value.

As can be seen from the model results for different initial exsolved volatile cases (shown in Supplementary Materials Figs S1-S4), S results are not sensitive to the volatile phase composition, due to the given solubility model. Because initial CO_2 concentrations are considerably lower than H_2O and S concentrations, its effect on the exsolved volatile phase composition is small. That leaves H_2O, which is the fastest diffusing species. We do not explicitly model the kinetics of water exsolution from the surrounding melt and, hence, its effect on the solubility boundary condition for the embayment diffusion calculation; however, a range of volatile compositions are taken into consideration by assessing a range of values for the initial mass of pre-existing exsolved volatiles. Model results indicate that this has a second order effect on decompression rate estimates. Given uncertainties in melt geometry surrounding the embayment bubble, modeling of volatile diffusion outside of the embayment is unlikely to provide significant improvement to our estimates.

The diffusion calculations proceeded from time $t = 0$ and $P(t = 0)$, equal to the pressure at which C_i^O are in equilibrium, at a constant dP/dt until a pressure of P_f is reached. Once $P = P_f$, the calculation was terminated and the resultant concentrations of H_2O, CO_2, and S, as a function of distance from embayment mouth (χ) was compared with the measured values using weighted least squares. In reality, it is likely that degassing continues for some time above the vent, probably for 10s of seconds and considerably less than magma decompression time. Although this would somewhat increase estimates of decompression rate, the effect will be of second order relative to degassing during ascent to the surface. Magma temperature was found using the olivine-liquid thermometer of Helz and Thornber (1987) and was assumed constant. Although the magma may undergo cooling of about 100 °C upon ascent (e.g., Sahagian and Proussevitch 1996; Mastin and Ghiorso 2001), the corresponding change in volatile diffusivity is approximately a factor of 1/2 for H_2O, CO_2, and S each (Freda

et al. 2005; Zhang et al. 2007, 2010). Because cooling will be most pronounced in the upper few hundred meters of the conduit, where most of the H_2O exsolves and vapor expansion is largest, the effect of cooling is likely no more or less than a factor of two on decompression-rate estimates.

We calculated the error between measured and predicted concentrations for each volatile species at points $\mathcal{X}_i$ as

$$\Psi_j = \frac{1}{\sum_i \alpha_{ji}} \sum_i \alpha_{ji} \left(C_{ji} - \hat{C}_{ji}\right)^2 \quad (2)$$

Where C_{ji} is the measured concentration of species j at location $\mathcal{X}_i$, $\hat{C}_{ji}$ the value predicted by the model, and α_{ji} is a value between 0 and 1. The combined RMS error was then calculated as

$$RMS\ \text{error} = \frac{1}{3}\sum_{j=1}^{3} \psi j \quad (3)$$

Each data point was given equal weight in order to minimize bias, that is $\alpha_{ji} = 1$ for all data, except H_2O for KeaE1 due to the very long plateau in the embayment interior. All three volatile species are thus also weighted equally. Although slightly improved best fits can be obtained by informed non-uniform data weighting, we refrained from doing so and, thus, provide the most transparent and objective estimates. However, for KeaE1, values of $\mathcal{X}_i$ were adjusted to account for the small secondary bubble that existed within the embayment. Furthermore, H_2O data were weighted to ensure all best-fit diffusion profiles to pass through the measured concentration at the embayment mouth. This does not significantly affect estimated decompression rates; it prevents fits at a high P_f to be considered, because these violate the strong observational constraint of H_2O concentration in the matrix glass. All independent parameters listed above were varied independently in a grid search. As expected, model fits to data are most sensitive to *dP/dt*. Initially, a coarse grid search was performed over a wide range in parameter values, in order to determine an optimal range of values subsequently used for a more refined grid search (ranges listed in Table 1). The entire analysis was performed for several values of M^0; they are 0.1, 0.2, 0.4, 0.8, 1.6, 3.2, and 6.4 wt.%. For each given M^0, a five-parameter grid search was performed, except for samples where it became evident from the pre-analysis that there is no need to vary the value of C_S^O, for which the grid search was only over four parameters. The results of the grid search for all the parameters for each embayment, which illustrate the model sensitivities, are shown in Supplementary Materials Fig. 1–4. For each embayment, there is a well-defined minimum in RMS error that constrains *dP/dt* to a distinct value for each eruption.

Decompression model results

Compositional profiles from the best-fitting diffusion models for H_2O, CO_2, and S from each embayment are shown in Fig. 3. To illustrate how decompression rate affects model results, each of the compositional plots in Fig. 3 also shows the results from models using the full range of decompression rates included in the grid search (gray lines in Fig. 3, values in Table 1). In addition, the first panel in each row illustrates how the RMS error for the models varies depending on the decompression rate and the mass of pre-existing exsolved volatiles. The final parameters used in each model are listed in Table 2.

For the embayment from episode 1 of the 1959 Kīlauea Iki eruption (IkiE1; Fig. 3a–d), a ~350-m high Hawaiian fountain, the shape of the profiles for H_2O and CO_2 suggests that diffusion has affected concentrations along the entire length of the embayment. Consistent with this observation, we obtain better-fitting models for initial concentrations greater than those observed in the embayment interior. To limit our modeling to realistic pre-eruptive H_2O contents, we therefore impose an upper limit on the initial H_2O concentration of 0.8 wt%, slightly above the maximum observed in melt inclusions from this eruption (and from Kīlauea in general, e.g., Wallace and Anderson 1998; Sides et al. 2014a). We find that the best-fitting ascent model is then obtained with an initial H_2O concentration of 0.75 ± 0.005 wt% (close to the maximum melt inclusion value), an initial CO_2 of 400 ± 100 ppm, and an initial S concentration of 1410 ± 20 ppm, with the latter similar to the maximum value measured in the embayment. In general, the addition of extra exsolved volatiles decreases the

Table 1 Range of parameters used in the grid search

Embayment	*dp/dt* (MPa)	C_{H2O}^O (wt%)	C_{CO2}^O (ppm)	C_S^O (ppm)	P_f *(MPa)*	M^0 (wt%)
IkiE1	0.02–0.07	0.6–0.8	300–1200	1390–1490	0.1–1.5	0.1–3.2
ReticE1	0.1–0.4	0.535–0.57	180–192.5	1300	0.25–11	0.1–6.4
ReticE2	0.02–0.4	0.57–0.63	167.5–192.5	1320	0.25–3.25	0.1–3.2
KeaE1	0.215–1.598	0.515–0.565	265–275	1420	0.25–6	0.1–3.2

Table 2 Parameters for best-fit diffusion-ascent models for each embayment

Embayment	*dp/dt* (MPa)	C^O_{H2O} (wt%)	C^O_{CO2} (ppm)	C^O_S (ppm)	P_f *(MPa)*	M^0 (wt%)	*T°C*
IkiE1	0.05 ± 0.005	0.75 ± 0.005	400 ± 100	1390 ± 20	0.1 ± 0.1	0.1	1192
ReticE1	0.32 ± 0.02	0.54 ± 0.005	182.5 ± 2.5	1300	2.75 ± 0.5	1.6	1163
ReticE2	0.1 ± 0.02	0.605 ± 0.005	167.5 ± 2.5	1320	2.75 ± 0.5	1.6–3.2	1163
KeaE1	0.45 ± 0.01	0.54 ± 0.05	265 ± 5	1420	2 ± 0.25	0.8	1160

Parameters shown are those that were found to minimize the RMS error between the model and the observed concentration profiles for each embayment based on the results of the grid search. See supporting information for further details. Modeled concentration profiles using these parameters are shown in Fig. 3

dp/dt decompression rate, C^O_{H2O}: initial H_2O, C^O_{CO2}: initial CO_2, C^O_S: initial sulfur, P_f final pressure, M^o mass of pre-existing exsolved volatiles

fit of the model to the data (Supplementary Materials Fig. S1), with the best-fitting model requiring only 0.1 wt%. The resulting decompression rate for this embayment is 0.05 MPa s^{-1}. Assuming that the magma is volatile saturated, the initial pressure for this embayment prior to eruptive ascent is 110 MPa (~4 km, assuming near-lithostatic pressure).

For the reticulite deposit (≥600 m high Hawaiian fountains), we present data for two embayments from separate crystals, one measured using NanoSIMS (ReticE1; Fig. 3i–l) and one using standard SIMS (ReticE2; Fig. 3e–h). Due to the larger uncertainties in measured concentrations and lower spatial resolution of the SIMS data, the results from this embayment are less certain compared with those measured by NanoSIMS but provide support for a coherent set of parameters for this eruption. Concentrations along both embayments are similar for all volatiles (Figs 3f–h and 3g–l), and both models have initial concentrations equivalent to the maximum measured values, as expected for longer embayments. Decompression models that match the measured profiles require the addition of ~2–3 wt% of pre-existing exsolved volatiles (Fig. 3e, i), which buffers CO_2 concentrations in the melt during initial ascent. This indicates pre-eruptive storage at 40 MPa (~1.5 km of lithostatic pressure). The presence of a significant mass of exsolved volatiles, presumably derived either from volatile exsolution within a deeper part of the volcanic system or by vapor/fluid accumulation via closed system exsolution in crustal chambers, is often proposed to play a significant role in basaltic eruptions (Allard et al. 2005; La Spina et al. 2015; Spilliaert et al. 2006; Vergniolle and Jaupart 1986). Geochemical evidence for this can theoretically be found in melt inclusions (e.g., Blundy et al. 2010), but such data are difficult to interpret. Because melt embayments record interactions between melt and exsolved volatiles during the final stage of ascent (i.e., from the magma reservoir to the surface), they provide a potential constraint on the presence of pre-existing or "excess" exsolved volatiles, assuming that the magma-fluid/vapor system outside the embayment is closed and representative of the erupting magma at large. Best-fit models for these embayments give decompression rates of 0.32 MPa s^{-1} (ReticE1) and 0.1 MPa s^{-1} (ReticE2).

The embayment from the most explosive of the three eruptions, the c. 1650 CE subplinian eruption of layer 6 (KeaE1; Fig. 3m-p), has distinct compositional plateaux for all volatiles in the embayment interior, which have similar concentrations to the initial concentrations in the model results. This suggests pre-eruptive storage at ~60 MPa (~2 km). The best-fitting model for this embayment also involves some pre-existing exsolved volatiles (~0.8 wt%) and gives the highest decompression rate of the embayments presented here of 0.45 MPa s^{-1}.

Discussion

A schematic illustration of the results of the embayment models for pre-eruptive volatile contents and decompression rates is shown in Fig. 4. The initial pressures of 40–60 MPa given by the embayments from the Reticulite and Layer 6 deposits translate to depths ~1.5–2 km. The vents for both these eruptions were located inside Kīlauea's summit caldera, and these storage depths are consistent with the inferred depth of the main sub-caldera reservoir (Poland et al. 2014). In contrast, the embayment from Kīlauea Iki ep. 1 gives a higher initial pressure of 110 MPa (~4 km depth) and therefore appears to reflect melts ascending from greater depths. The 1959 Kīlauea Iki vent was located on the rim of the caldera (Fig. 1), which is not the case for most summit eruptions and implies a somewhat different ascent path. If these melts were fed through the sub-caldera reservoir, for example, as suggested by Poland et al. (2014), this does not appear to have affected exsolution of CO_2, implying minimal interaction with any resident magma. Ascent timescales based on our average decompression rates vary from ~2–7 min for the c. 1500 reticulite and c. 1650 Layer 6 eruptions to ~36 min for the Kīlauea Iki ep. 1 eruption, with average velocities during ascent of ~5–10 m s^{-1} and ~2 m s^{-1}, respectively. For the two Hawaiian style eruptions (Reticulite and Kīlauea Iki), exit

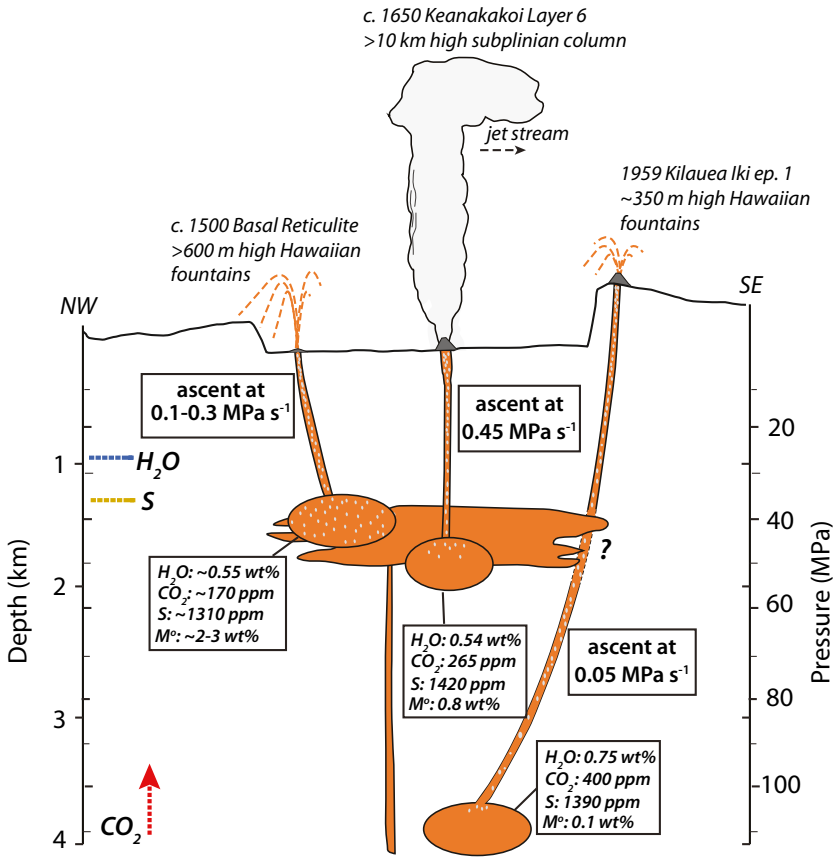

Fig. 4 Schematic illustration of the ascent conditions and pre-eruptive volatile contents for explosive eruptions at Kīlauea's summit caldera constrained by the embayment models. The initial dissolved volatile concentrations in the embayment melt prior to ascent are shown at the base of each column along with the mass of co-existing exsolved volatiles (M^o). Although the pathway for the Kīlauea Iki magma is inferred to pass through the summit storage region (based on more recent geophysical data), the embayment model suggests that the magma erupted during this part of the eruption was sourced from greater depths. The interaction of this melt with the caldera storage region is unclear and it did not appear to affect the exsolution of CO_2. For all eruptions, pre-eruptive storage occurs at pressures where the magma is volatile saturated and the embayment melt is therefore considered to have equilibrated with a co-existing CO_2-rich fluid. *Colored lines* show where each volatile species starts to significantly exsolve/diffuse. Depth is estimated assuming a lithostatic gradient with a crustal density of 2850 kg m^3. The simplified plumbing system shown is to illustrate the constraints on ascent given by the embayment models and does not reflect the actual complexities of melt storage beneath Kīlauea (e.g., see Poland et al. 2014)

velocities at the vent based on these decompression rates are consistent with the observed/inferred fountain heights.

Our diffusion modeling gives average decompression rates of ~0.05 and ~0.1–0.3 MPa s^{-1} for the ~350 m and ≥600 m high Hawaiian fountain eruptions, respectively. The embayment from the larger subplinian size eruption gives a higher rate of ~0.45 MPa s^{-1}, comparable to those for a subplinian eruption from a wet (~4 wt% H_2O) basaltic andesite arc volcano (0.39 ± 0.07 MPa s^{-1}, the average of four embayments from the October 17, 1974 eruption of Volcan Fuego, Guatemala; Lloyd et al. 2014) (Fig. 5). The products of the subplinian eruption (Keanakako'i tephra layer 6) are observed to be significantly more microlite-rich than those of the two less-intense fountaining events, and this may have influenced the ability of gas to segregate and escape from the ascending magma due to rheological changes (e.g., Sable et al. 2006; Wright et al. 2012). It is notable that the c. 1500 reticulite seems to have involved the greatest mass of pre-existing exsolved volatiles. It remains unclear whether this was of significance in producing such a reticulite-rich deposit, and it has been suggested that faster melt ascent rates will increase coupling between melts and exsolved volatiles and therefore porosity (e.g., Mangan et al. 2014). In general, however, there is no obvious link between the mass of pre-existing volatiles and eruption magnitude. In addition, the lack of evidence for a correlation between pre-eruptive volatile content and eruption magnitude, for example, as recently proposed for Kīlauea by Sides et al. (2014b), does not favor the concept that variations in initial volatile concentrations are the drivers for variability in eruptive style. In fact, the least intense eruption (Kīlauea Iki ep. 1) appears to have involved the magma with the highest initial volatile inventory.

Overall, the Kīlauea embayments record average decompression rates that increase with eruption magnitude/discharge rate (Fig. 5). When compared with embayment data from other basaltic-andesitic (Fuego; Lloyd et al. 2014) and silicic

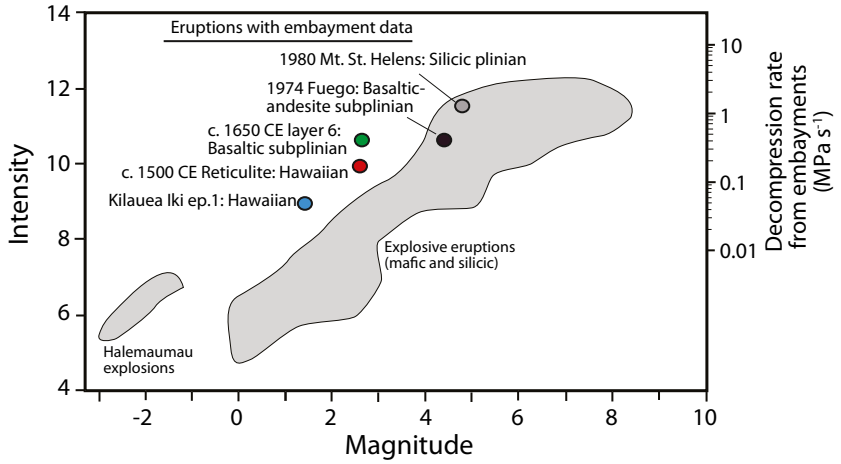

Fig. 5 Comparison between eruptive intensity, magnitude, and decompression rate for eruptions with melt embayment data. Also shown in the *gray fields* are eruptive magnitude and intensity for a compilation of explosive eruptions by Pyle (2015). The decompression rate axis only applies to the labeled data points, which all have decompression rates calculated via embayment diffusion studies. These record average decompression rates that vary by three orders of magnitude for eruptions ranging in size from Hawaiian fountains to a plinian event. The eruptive intensity for these events has a range of around four orders of magnitude, implying a non-linear relationship between these parameters. Embayment results from Liu et al. (2007) are not plotted due to the much coarser spatial resolution of the FTIR analysis used in that study

(Mt. St. Helens; Humphreys et al. 2008) eruptions, a general trend of increasing decompression rate is mirrored by increases in eruptive intensity and, more weakly, magnitude. These different studies record average decompression rates that vary over approximately two orders of magnitude for eruptions ranging over almost four orders of magnitude in intensity, from Hawaiian fountains to Plinian eruptions. This non-linear relationship between intensity and decompression rate is intriguing and probably a consequence of significant differences in the hydrostatic and viscous contributions to the overall rate of decompression. The weaker correlation between decompression rate and magnitude is expected, since variations in conduit geometry are unlikely to be strongly controlled by pre-eruptive magma volume.

Conclusion

Magma decompression is a key process that modulates the kinetics of bubble nucleation, growth, and coalescence, which in turn affects volatile exsolution and the potential for explosive activity (e.g., Parfitt and Wilson 1995, 1999; Cashman 2004; Parfitt 2004). This study presents the first independent quantitative observational constraints on magma decompression rates, and thereby indirectly ascent rates, during explosive basaltic eruptions. Our results demonstrate that this method is well suited to basaltic systems and future work at Kīlauea and other volcanoes can expand the current database of embayment analyses, allowing for a greater understanding of how this parameter varies between different eruptions. The embayment method has the potential to provide well-constrained information not only on ascent conditions but potentially on the presence of pre-existing exsolved volatiles at the onset of eruptive ascent. As demonstrated here, and also by Lloyd et al. (2014), the NanoSIMS technique provides an important new tool for constraining compositional gradients of multiple volatile species at spatial scales relevant to volatile diffusion in silicate melts. Our results provide the first constraints from Hawaii with which to develop dynamic conduit flow models and to test inferences from the textural analysis of eruption deposits (e.g., Mangan and Cashman 1996; Stovall et al. 2011) for how decompression rate influences volatile exsolution and magma fragmentation.

Acknowledgments This work was supported by NSF grant (EAR1145159). H.G. was supported by NSF grant EAR1145187. D.J.F. also acknowledges support from a Lamont-Doherty Postdoctoral Fellowship and P.R. from NSF grants EAR1348022 and EAR1426820. We are grateful to Julianne Gross at AMNH for assistance with the electron microprobe analysis, Alex Lloyd for discussions and lab support, and Jacob Lowenstern and Mike Poland for comments on an earlier version of the paper. We acknowledge reviews by Nicole Metrich and two anonymous reviewers.

References

Allard P, Burton M, Muré F (2005) Spectroscopic evidence for a lava fountain driven by previously accumulated magmatic gas. Nature 433:407–410. doi:10.1038/nature03246

Blundy J, Cashman KV, Rust A, Witham F (2010) A case for CO2-rich arc magmas. Earth. Planet. Sci Lett 290:289–301. doi:10.1016/j.epsl.2009.12.013

Cashman KV (2004) Volatile controls on magma ascent and eruption, in The State of the Planet: Frontiers and Challenges in Geophysics

Geophys. Monogr. Ser., Vol. 150. edited by Sparks RSJ, Hawkesworth CJ 109–124, doi: 10.1029/150GM10
Cashman KV, Sparks RSJ (2013) How volcanoes work: a 25 year perspective. GSA Bull 125:664–690. doi:10.1130/B30720.1
Castro JM, Dingwell DB (2009) Rapid ascent of rhyolitic magma at Chaitén volcano, Chile. Nature 461:780–783. doi:10.1038/nature08458
Costa F, Dungan M (2005) Short time scales of magmatic assimilation from diffusion modeling of multiple elements in olivine. Geology 33:837–840. doi:10.1130/G21675.1
Dixon J (1997) Degassing of alkalic basalts. Am Mineral 82(368–378):1997
Eaton JP, Richter DH, Krivoy HL (1987) Cycling of magma between the summit reservoir and Kīlauea Iki lava lake during the 1959 eruption of Kīlauea Volcano, in Volcanism in Hawai'i, USGS Prof. Paper. 1350 edited by Decker, RW, Wright TL, Stauffer PH 307–1335.
Freda C, Baker DR, Scarlato P (2005) Sulfur diffusion in basaltic melts. Geochim Cosmochim Acta 69(5061–5069):2005. doi:10.1016/j.gca.2005.02.002
Goepfert K, Gardner J (2010) Influence of pre-eruptive storage conditions and volatile contents on explosive Plinian style eruptions of basic magma. Bull Volcanol 72(5):511–521
Gonnermann HM (2015) Magma fragmentation. Annu Rev Earth Planet Sci 43:431–458. doi:10.1146/annurev-earth-060614-105206
Gonnermann HM, Manga M (2005) Nonequilibrium magma degassing: results from modeling of the ca. 1340 AD eruption of Mono Craters, California. Earth Planet Sci Lett 238:1–16. doi:10.1016/j.epsl.2005.07.021
Gonnermann HM, Manga M (2007) The fluid mechanics inside a volcano. Annu Rev Fluid Mech 39(1):321–356
Hauri EH, Weinreich T, Saal AE, Rutherford MC, Van Orman JA (2011) High pre-eruptive water contents preserved in lunar melt inclusions. Science 333:213–215. doi:10.1126/science.1204626
Helz RT, Thornber CR (1987) Geothermometry of Kilauea Iki lava lake. Hawaii Bull Volc 49:651–668
Houghton BF, Gonnermann HM (2008) Basaltic explosive volcanism: constraints from deposits and models. Chem Erde-Geochem 68:117–140. doi:10.1016/j.chemer.2008.04.002
Humphreys MCS, Menand T, Blundy JD, Klimm K (2008) Magma ascent rates in explosive eruptions: constraints from H2O diffusion in melt inclusions. Earth. Planet. Sci Lett 270:25–40. doi:10.1016/j.epsl.2008.02.041
La Spina A, Burton M, Allard P, Alparone S, Muré F (2015) Open-path FTIR spectroscopy of magma degassing processes during eight lava fountains on Mount Etna. Earth. Planet. Sci Lett 413:123–134. doi:10.1016/j.epsl.2014.12.038
Lensky NG, Navon O, Lyakhovsky V (2004) Bubble growth during decompression of magma: experimental and theoretical investigation. J Volcanol Geotherm Res 129:7–22. doi:10.1016/S0377-0273(03)00229-4
Liu Y, Anderson AT, Wilson CJN (2007) Melt pockets in phenocrysts and decompression rates of silicic magmas before fragmentation. J Geophys Res 112:B06204. doi:10.1029/2006JB004500
Lloyd AS, Ruprecht P, Hauri EH, Rose W, Gonnerman H, Plank T (2014) NanoSIMS results from olivine-hosted melt embayments: magma ascent rate during explosive basaltic eruptions. J Volcanol Geotherm Res 283:1–18. doi:10.1016/j.jvolgeores.2014.06.002
Mangan MT, Cashman KV (1996) The structure of basaltic scoria and reticulite and inferences for vesiculation, foam formation, and fragmentation in lava fountains. J Volcanol Geotherm Res 283:73(1):1–18. doi:10.1016/0377-0273(96)00018-2
Mangan MT, Cashman KV, Swanson DA (2014) The dynamics of Hawaiian-style eruptions: a century of study, in Characteristics of Hawaiian Volcanoes edited by Poland MP, Takahashi TJ, Landowski CM USGS Prof. Paper, 1801, doi: 10.3133/pp18018
Mastin LG (2002) Insights into volcanic conduit flow from an open-source numerical model. Geochem Geophys Geosyst 3:7. doi:10.1029/2001GC000192
Mastin LG, Ghiorso MS (2001) Adiabatic temperature changes of magma–gas mixtures during ascent and eruption. Contrib Min Pet 141(3):307–321
May M, Carey RJ, Swanson DA, Houghton BF (2015) Reticulite-producing fountains from ring fractures in Kīlauea Caldera ca. 1500 CE, in Hawaiian Volcanoes: From Source to Surface edited by R. Carey, V. Cayol, M. Poland and D. Weis, pp. 351–367, doi: 10.1002/9781118872079.ch16
McPhie J, Walker GPL, Christiansen RL (1990) Phreatomagmatic and phreatic fall and surge deposits from explosions at Kīlauea Volcano, Hawai'i, 1790 A.D.: Keanakakoi Ash Member. Bull. Volc 52:334–354. doi:10.1007/BF00302047
Namiki A, Manga M (2006) Influence of decompression rate on the expansion velocity and expansion style of bubbly fluids. J Geophys Res 111:B11. doi:10.1029/2005JB004132
Namiki A, Manga M (2008) Transition between fragmentation and permeable outgassing of low viscosity magmas. J Volcanol Geotherm Res 169:48–60. doi:10.1016/j.jvolgeores.2007.07.020
Newman S, Lowenstern JB (2002) VOLATILECALC: a silicate melt–H2O–CO2 solution model written in visual basic for excel. Comput Geosci 28:597–604. doi:10.1016/S0098-3004(01)00081-4
Parcheta C, Fagents S, Swanson DA, Houghton BF, Ericksen T (2015) Hawaiian fissure fountains: quantifying vent and shallow conduit geometry, Episode1 of the 1969–1974 Mauna Ulu Eruption In Hawaiian Volcanoes: From Source to Surface Geophys. Monogr. Ser., vol. 208, edited by Carey R, Cayol V, Poland M, Weis D 369–391, doi: 10.1002/9781118872079.ch16
Parfitt EA (2004) A discussion of the mechanisms of explosive basaltic eruptions. J Volcanol Geotherm Res 134:77–107. doi:10.1016/j.jvolgeores.2004.01.002
Parfitt EA, Wilson L (1995) Explosive volcanic eruptions—IX. The transition between Hawaiian-style and lava fountaining and Strombolian explosive activity. Geophys J Int 121:1. doi:10.1111/j.1365-246X.1995.tb03523.x
Parfitt EA, Wilson L (1999) A Plinian treatment of fallout from Hawaiian lava fountains. J Volcanol Geotherm Res 88:67–75. doi:10.1016/S0377-0273(98)00103-6
Pichavant M, Di Carlo I, Rotolo SG, Scaillet B, Burgisser A, Le Gall N, Martel C (2013) Generation of CO2-rich melts during basalt magma ascent and degassing. Contrib Min Petrol 166(2):545–561. doi:10.1007/s00410-013-0890-5
Poland MP, Miklius A, Montgomery-Brown EK (2014) Magma supply, storage, and transport at shield-stage. In Characteristics of Hawaiian Volcanoes, USGS Prof. Paper 1801, edited by Poland MP, Takahashi TJ, Landowski CM, doi: 10.3133/pp18015
Proussevitch AA, Sahagian DL, Anderson AT (1993) Dynamics of diffusive bubble growth in magmas: isothermal case. J Geophys Res 98(22283–22307):1993. doi:10.1029/93JB02027
Pyle DM (2015) Sizes of volcanic eruptions, In Encyclopedia of Volcanoes 2nd Edition edited by Sigurdsson, H., B. Houghton., S. McNutt., H. Rymer., H. and J. Stix. pp. 257–264, Elsevier.
Ruprecht P, Plank T (2013) Feeding andesitic eruptions with a high-speed connection from the mantle. Nature 500:68–72. doi:10.1038/nature12342
Rutherford MJ, Hill PM (1993) Magma ascent rates from amphibole breakdown: experiments and the 1980- 1986 Mount St. Helens eruptions. J Geophys Res 98:19667–19685. doi:10.1029/93JB01613
Saal AE, Hauri EH, Cascio MJ, Van Orman JA, Rutherford MC, Cooper RF (2008) Volatile content of lunar volcanic glasses and the presence of water in the Moon's interior. Nature 454:192–195. doi:10.1038/nature07047
Sable JE, Houghton BF, Del Carlo P, Coltelli M (2006) Changing conditions of magma ascent and fragmentation during the Etna 122 BC basaltic Plinian eruption: evidence from clast microtextures. J

Volcanol Geotherm Res 158:333–354. doi:10.1016/j.jvolgeores.2006.07.006

Sahagian DL, Proussevitch AA (1996) Thermal effects of magma degassing. J Volcanol Geotherm Res 74(1)

Sides I, Edmonds M, Maclennan J, Houghton BF, Swanson DA, Steele-MacInnis MJ (2014a) Magma mixing and high fountaining during the 1959 Kīlauea Iki eruption, Hawai 'i. Earth Planet Sci Lett 400: 102–112

Sides IR, Edmonds M, Maclennan J, Swanson DA, Houghton BF (2014b) Eruption style at Kīlauea Volcano in Hawai'i linked to primary melt composition. Nat Geosci 7:464–469. doi:10.1038/ngeo2140

Spilliaert, N., P. Allard, N Métrich, and A V. Sobolev (2006), Melt inclusion record of the conditions of ascent, degassing, and extrusion of volatile-rich alkali basalt during the powerful 2002 flank eruption of Mount Etna (Italy), J. Geophys. Res., 111, B04203, doi:10.1029/2005JB003934.

Stovall WK, Houghton BF, Gonnermann H, Fagents SA, Swanson DA (2011) Eruption dynamics of Hawaiian-style fountains: the case study of episode 1 of the Kīlauea Iki 1959 eruption. Bull. Volc 73: 511–529. doi:10.1007/s00445-010-0426-z

Suzuki Y, Fujii T (2010) Effect of syneruptive decompression path on shifting intensity in basaltic sub-Plinian eruption: implication of microlites in Yufune-2 scoria from Fuji volcano, Japan. J Volcanol Geotherm Res 198:158–176. doi:10.1016/j.jvolgeores.2010.08.020

Swanson DA, Rose TR, Fiske RS, McGeehin JP (2012) Keanakakoi Tephra produced by 300 years of explosive eruptions following collapse of Kīlauea's caldera in about 1480 CE. J Volcanol Geotherm Res 215:8–25. doi:10.1016/j.jvolgeores.2011.11.009

Swanson DA, Rose TR, Mucek AE, Garcia MO, Fiske RS, Mastin LG (2014) Cycles of explosive and effusive eruptions at Kīlauea Volcano, Hawai 'i. Geology 42(7):631–634. doi:10.1130/G35701.1

Toramaru A, Noguchi S, Oyoshihara S, Tsune A (2008) MND (microlite number density) water exsolution rate meter. J Volcanol Geotherm Res 175:156–167. doi:10.1016/j.jvolgeores.2008.03.035

Vergniolle S, Jaupart C (1986) Separated two-phase flow and basaltic eruptions. J Geophys Res 91:12842–12860. doi:10.1029/JB091iB12p12842

Wallace PJ, Anderson AT Jr (1998) Effects of eruption and lava drainback on the H2O contents of basaltic magmas at Kīlauea Volcano. Bull Volc 59(5):327–344. doi:10.1007/s004450050195

Wilson L, Head JW (1981) Ascent and eruption of basaltic magma on the Earth and Moon. J Geophys Res 86:2971–3001. doi:10.1029/JB086iB04p02971

Witham F, Blundy J, Kohn SC, Lesne P, Dixon J, Chirakov SV, Botcharnikov R (2012) SolEx: a model for mixed COHSCl-volatile solubilities and exsolved gas compositions in basalt. Comput Geosci 45:87–97. doi:10.1016/j.cageo.2011.09.021

Woods AW (1995) The dynamics of explosive volcanic eruptions. Revs Geophys 33(495):530. doi:10.1029/95RG02096

Wright HM, Cashman KV, Mothes PA, Hall ML, Ruiz AG, Le Pennec JL (2012) Estimating rates of decompression from textures of erupted ash particles produced by 1999–2006 eruptions of Tungurahua volcano, Ecuador. Geology 40:619–622. doi:10.1130/G32948.1

Zhang Y, Xu Z, Zhu M, Wang H (2007) Silicate melt properties and volcanic eruptions. Rev Geophys 45(27):2007. doi:10.1029/2006RG000216

Zhang Y, Ni H, Chen Y (2010) Diffusion data in silicate melts. Rev Mineral Geochem 72:311–408. doi:10.2138/rmg.2010.72.8